Laser and Particle Beams (2015), *33*, 59–64.

doi:10.1017/S0263034614000779

A setup for studies of laser-driven proton acceleration at the Lund Laser Centre

B. AURAND,[1] M. HANSSON,[1] L. SENJE,[1] K. SVENSSON,[1] A. PERSSON,[1] D. NEELY,[2] O. LUNDH,[1] AND C.-G. WAHLSTRÖM[1]

[1]Department of Physics, Lund University, Lund, Sweden
[2]Central Laser Facility, STFC Rutherford Appleton Laboratory, Didcot, United Kingdom

(RECEIVED 8 September 2014; ACCEPTED 26 October 2014)

Abstract

We report on a setup for the investigation of proton acceleration in the regime of target normal sheath acceleration. The main interest here is to focus on stable laser beam parameters as well as a reliable target setup and diagnostics in order to do extensive and systematic studies on the acceleration mechanism. A motorized target alignment system in combination with large target mounts allows for up to 340 shots with high repetition rate without breaking the vacuum. This performance is used to conduct experiments with a split mirror setup exploring the effect of spatial and temporal separation between the pulses on the acceleration mechanism and on the resulting proton beam.

Keywords: Laser-ion acceleration; Mirror design; Radiation detectors

INTRODUCTION

Within the last decade, tremendous progress has been made in the field of laser ion acceleration. First demonstrated *Wilks et al.*, 2001 by the mechanism of target normal sheath acceleration (TNSA) nowadays provides a source for ultra-short proton bunches with energies up to several tens of MeV (Daido *et al.*, 2012; Passoni *et al.*, 2010). An ultra-intense laser pulse ($I > 10^{16}$ W/cm^2) which interacts with the front-side of a μm-thick target foil drives a massive electron current toward the rear-side of the target. The electrons exiting the target on the scale of the Debye-length create a charge separation field between them and the positively charged remaining bulk. This generates an electric field in the order of a few TV/m. In this field, which can be considered static on the timescale of a several 100's of fs up to a few ps (Schreiber *et al.*, 2006), protons and heavier ions like carbon or oxygen — mainly from the hydrocarbon contamination layer on the target — are accelerated.

Numerous studies on the mechanism of TNSA have been made so far, e.g., the investigation of the dependence on laser parameters like the focal spot size (Brenner *et al.*, 2011), energy (Coury *et al.*, 2012), or pulse duration (Robson *et al.*, 2007), studies on the electron current driven in the target (Tresca *et al.*, 2011; Coury *et al.*, 2013), or different target geometry (Schwoerer *et al.*, 2006; Ramakrishna *et al.*, 2010; Hegelich *et al.*, 2006; Burza *et al.*, 2011). In our current study on TNSA acceleration, we focus on the influence of two independent laser pulses with different temporal and spatial separation, interacting with the target and driving the acceleration. In this paper we describe the technical part of the setup, which includes laser and particle diagnostics as well as the target and optical probing system.

Address correspondence and reprint request to Bastian Aurand, Department of Physics, Lund University, 22100 Lund, Sweden.
E-mail: bastian.aurand@uni-duesseldorf.de

LASER SYSTEM

The Lund terawatt laser is a Ti:Sapphire based CPA (Strickland & Mourou, 1985) laser system with four amplification stages situated in the basement of the Physics Department at Lund university. A dedicated diagnostic table setup next to the compressor allows the verification of the laser beam parameters on a daily basis. The pulse duration is measured with a second order single-shot autocorrelator. A third order scanning autocorrelator (Amplitude, Sequoia®) is used to measure the laser contrast. Besides that, the spectrum (RGB, Qwave®) and the spectral phase (Avesta, SPIDER SP-120) are recorded. A mirror in the beam line with a designed leakage of 1.5% allows for on-shot recording of autocorrelation and laser spectrum. Typical pulse parameters are an energy $E_L = 0.9$ J at a pulse duration of $\tau_L = 35$ fs. The laser contrast is $0.5–1 \times 10^{-9}$ up to 50 ps before the main

pulse. A beam position system controls piezo mirrors in the amplifier chain and compensates for long term drifts which helps to keep laser parameters stable during operation.

A deformable mirror (DM) with a clear aperture of 65 mm, segmented in 32 piezo controlled areas (NightN Ltd., DM2-65-32) in the beam line enables corrections of the wavefront downstream. The 45 mm diameter beam is guided in vacuum and can be delivered into two different target areas by flipping one of the beam line mirrors. One of the target areas is mainly dedicated to laser wakefield acceleration (LWFA) (Desforges *et al*., 2014; Hansson *et al*., 2014) experiments, whereas the other target area mainly for proton experiments. The radiation shielding allows simultaneous experiments on electrons in one room and preparation of ion acceleration experiments in the other room. Both cylindrical experimental chambers with an inner diameter of 108 cm and a height of 37 cm are accessible by removing the lid or flanges on the side of the vacuum vessel. In the following, we will focus on the proton setup only (Fig. 1).

TARGET SYSTEM

Below the proton chamber is a housing containing an electrically insulated and Faraday-shielded xyz-linear stage system (Newport, GTS70). Using optical encoded position sensors and double-shielded cables, malfunction events due to electro-magnetic pulses do not occur. All stages have a travel range of 70 mm at a velocity of up to 50 mm/s with an on-axis accuracy of ±1μm and a bi-directional position reproducibility of 100 nm. The upper part of the target mount holds a three-point load, multi-purpose holder on which different kinds of self-centering targets can be mounted. Additional tip/tilt screws enable target adjustments perpendicular to the motion axis which is checked for every target with a micrometer caliper. Primarily used is an matrix target mount with 340 (17 × 20) independent target positions of 1 mm diameter and 2.5 mm separation (Fig. 2a). The mount consists of two comb shaped plates where a target foil can be clamped in between (Fig. 2b). Using an additional spacer, double layered target configurations or grids for proton imaging purposes can be realized.

The position of the target chamber center (TCC) which is the dedicated focus position is defined by the overlap of two external lasers beams, each referenced to the center of two opposed flanges on the chamber wall. This position is transferred to an alignment needle on the target mount and verified during major rebuilds. The target is aligned in the TCC using the laser focus diagnostic, observing the

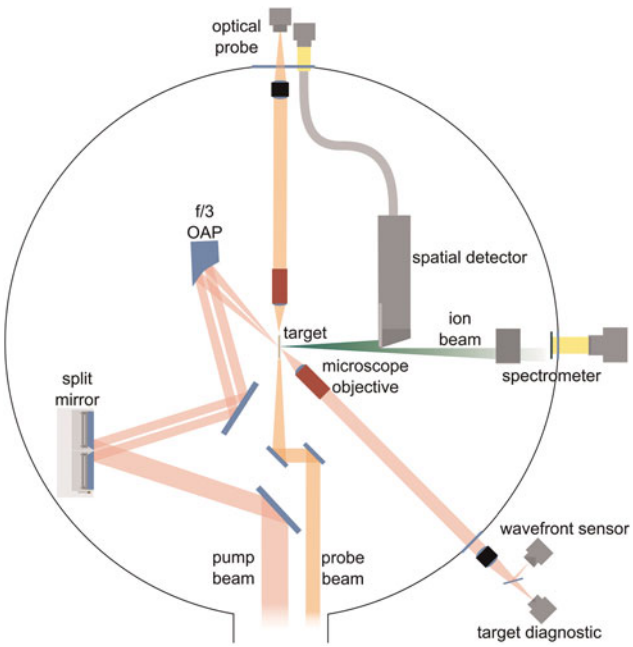

Fig. 1. Experimental setup for proton acceleration in the TNSA regime. The incident laser pulse is divided by a split-mirror into two beams which can be spatially and temporally shifted with respect to each other. Both beams are focused by the same OAP onto the target. The accelerated protons can be sent to a spectrometer for an energy measurement or a spatial detector in order to determine the beam profile. An independent optical probe can be used to do shadowgraphy or interferometry of the target rear surface.

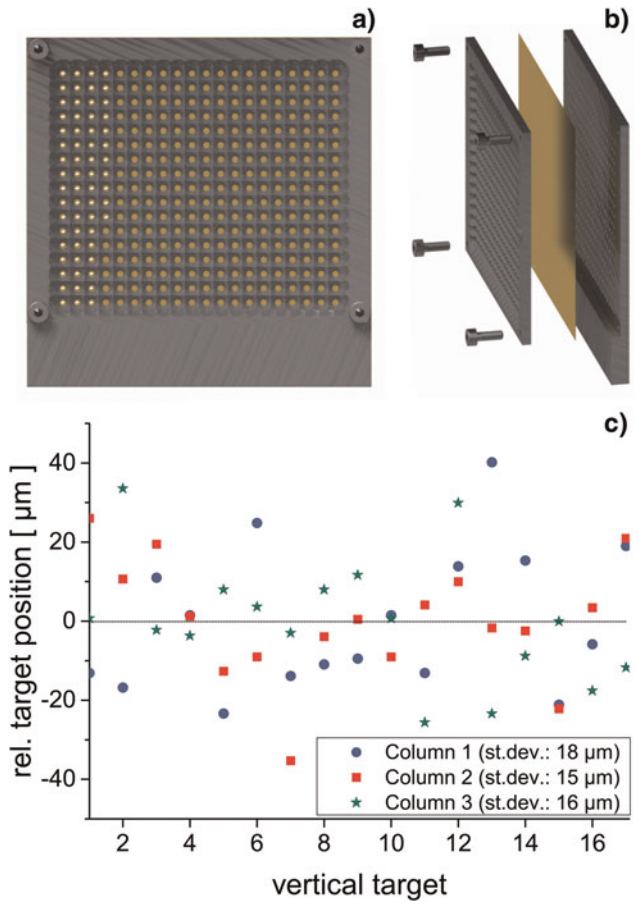

Fig. 2. (**a**) Matrix target mount with 340 (17 × 20) independent target positions. (**b**) The mount consists of two comb shaped plates in where the target foil is clamped in between (**c**) Scan of the relative focal position for a column wise vertical movement of a 3 μm Al foil. The standard deviation in each column is less than 18 μm.

https://doi.org/10.1017/S0263034614000779 Published online by Cambridge University Press

reflection of a monochromatic light source from the target rear surface at an angle of 45°. This diagnostic is based on an infinity corrected 10× objective (Mitutoyo, Plan Apo NIR) with a working distance of 31 mm, imaging the laser focal plane onto a camera outside the vacuum vessel. Alternatively, for the laser alignment, the beam can be sent to a modified Hartmann sensor (Hartmann, 1900; Primot *et al.*, 1995) (Phasics, SID4) to measure the wavefront. Note that within this setup using a DM, wavefront corrections for all optical elements up to the final focusing parabola can be included. The small depth of the focus diagnostic (4.1 μm) and the additional observation angle allow for a position accuracy of 2–3 μm with respect to the objective.

The typical procedure in order to take a series of shots is a columnwise pre-inspection of the target, regarding foil condition and possible wrinkles. This allows for a burst-mode of up to 17 shots within 1 min by moving the target vertically to the next position without any further inspection. Measurements of the focus position (Fig. 2c) for a pre-aligned target show a deviation of less than 18 μm, which is significantly smaller than the Rayleigh-length. This deviation is mainly given by imperfections during manufacturing of the target mount. The complete remote control of the target alignment enables a scan with a complete target in less than 1.5 h. Simultaneous monitoring and controlling of the laser parameters guarantee stable laser conditions. Further automated control of the target system, e.g., by target positioning via chromatic-confocal sensing (Ruprecht, A.K. *et al.* 2005) could increase the repetition rate and precision of the alignment.

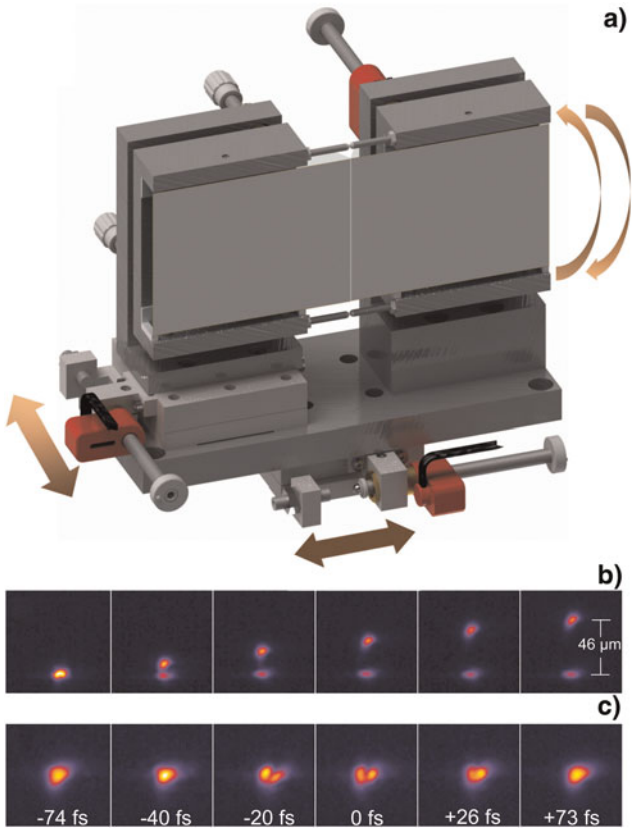

Fig. 3. (**a**) Split mirror setup generating two independent beams, which can be spatially and temporally shifted against each other. In addition the amount of energy in both parts can be changed. (**b**) Vertical focus separation by movement of one beam. (**c**) Interference structures are visible when the beams overlap within $\Delta t = \pm 20$ fs relative timing.

SPLIT MIRROR SETUP

Focusing of the laser is done by an off-axis parabolic mirror with 152 mm focal length (SORL, OAP 06-02-03/MMOA-3) giving a focal spot of 5 μm (FWHM) corresponding to a maximum intensity of 2×10^{19} W/cm^2 on the target and a measured Rayleigh-length of ($z_R \approx 50$ μm). One of the mirrors inside the experimental chamber consists of a specially designed split-mirror to generate two independent beams which can be spatially and temporally shifted with respect to each other (Fig. 3a). The setup is based on two protected silver mirrors sized 70×90 mm which have a thin edge to place them side by side, leaving a vertical gap of only a few tenths of a millimetre. Both mirrors are mounted separately and can be tilted horizontally and vertically using piezo-linear actuators (Newport, Picomotor). In addition, one of the mirrors is mounted on a linear stage allowing for a translation perpendicular to its surface. The introduced path difference of up to 20 mm in either direction at an incidence angle of ≈12° correspondes to a temporal delay of max. ±68 ps with respect to the fixed pulse. Finally, both mirrors can be moved sideways simultaneously to change the fraction of the incident beam on each mirror and therefore the energy ratio between the two pulses.

We deduce the minimal vertical movement of the beam in the focal plane to 150 nm/steps of the piezomotor tilting the mirror. In the given geometry, a vertical separation does not significantly change the length of each beam path, so it is not changing the relative timing between the two pulses. The bidirectional repeatability due to hysteresis effects in the mount is in the order of 5–6 μm. To avoid this effect, scans are always performed in one direction of movement (Fig. 3b).

The temporal overlap of the pulses is verified by the observation of an interference structure while both beams are spatially overlapped. The interference pattern is visible within a spatial range of 20 μm corresponding to ≈60 fs temporal range, showing a symmetric maximum (Fig. 3c). This method allows for a relative timing with a sub-pulse duration accuracy which is higher compared to methods like transverse probing of the generated plasma (Aurand *et al.*, 2014).

Advantageous for all kinds of measurement series done with this setup are the common beam line and the focusing system downstream of the split-mirror, making the measurements insensitive to beam pointing fluctuations. Even if the absolute focus position of the system undergoes a small spatial jitter, the relative spatial and temporal separation of the beams remained fixed.

https://doi.org/10.1017/S0263034614000779 Published online by Cambridge University Press

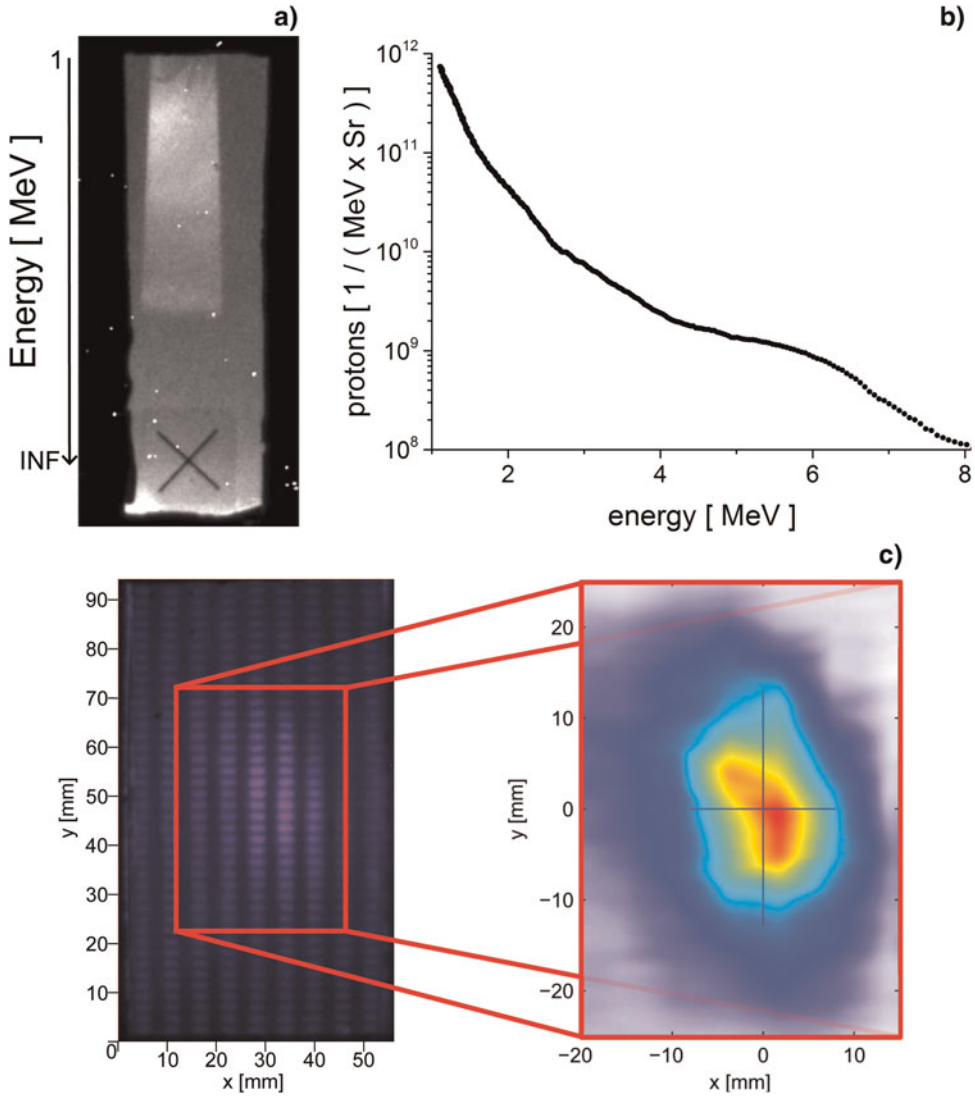

Fig. 4. Proton energy measurement from a 3 μm Al foil. (**a**) The raw data image obtained by the fluorescence of energy dispersed protons in a BC-408 scintillator in target normal direction. (**b**) Evaluated proton spectra using the calculated deflection curve and a cross calibration with CR-39 to get the absolute particle number. (**c**) Using the spatial detector, a beam profile of the accelerated particles can be taken. An Al filter grid in front of the detector allows for the subtraction of the electron background and a reconstruction of the proton beam profile.

ION DIAGNOSTIC

Ions are accelerated from the target rear surface. In order to be able to match the high repetition rate and the high number of shots per target, all diagnostics used in this setup have digital readouts.

The proton energy is determined by deflection of the proton beam in a magnetic field with an effective strength of $B_{Eff} = 0.69$ T and a length of 6 cm, which is situated in the target normal direction (47 ± 0.5) cm behind the target. A 1 mm horizontal entrance slit covers a solid angle of (8×10^{-5}) sr. Heavier ions are blocked by a 6 μm Al filter in front of the scintillator (St. Gobain, BC-408). The fluorescence signal is imaged by a 16-bit camera (Princeton, "PhotonMAX 1024")(Fig. 4a). To obtain the absolute particle number, a cross-calibration using a CR-39 trace detector was done (Cartwright *et al.*, 1978) (Fig. 4b). The lowest detectable energy, determined by the setup geometry, is 1.2 MeV. The highest resolvable energy is ≈10 MeV.

The proton beam profile is measured by moving a scintillator (St. Gobain, BC-408) with a thickness of 500 μm into to the beam at a position of (65 ± 2) mm behind the target. The scintillator is placed in a light-shielded aluminum box with a 12 μm thick Al entrance window and an acceptance angle of 28°. The scintillator is imaged by an objective inside the box onto an optical fiber bundle, which transfers the signal out of the vacuum chamber onto a camera (Fig. 4c). Using a grid of Al bars with different thicknesses in front of the scintillator allows for an analytical subtraction of the electron background, superimposed with the signal, by taking the different stopping power for electrons and protons into account. In

https://doi.org/10.1017/S0263034614000779 Published online by Cambridge University Press

contrast to a stack of radiochromic film (RCF), the energy selectivity of the scintillator is not very high. The signal is a superposition of all protons which are passing the filter and thus being transmitted or being stopped in the scintillator (d_{Scint} = 0.5 mm; 0.9 MeV ≤ E_{Stop} ≤ 7 MeV). In the future, a stack of scintillators with various thickness which are fluorescing at different wavelengths could be used to obtain an energy resolved signal (Green *et al*., 2011). Note that the response from a scintillator depends both on particle number and particle energy, which needs to be taken into account calculating absolute particle numbers (Green *et al*., 2011).

OPTICAL PROBE SETUP

A small amount (≈10 mJ) of the stretched pulse can be coupled from the last amplification stage of the laser system and sent to a separate pulse compressor. This part is compressed to roughly 60 fs and can optionally be frequency doubled ($\lambda_{2\omega}$= 400 nm). A specially designed curved target mount allows for probing along the target rear surface without being affected by the bright plasma on the front surface (Fig. 5a). A motorized linear stage with 150 mm travel enables controlled delay scans in a time window of up to 1 ns. The probe imaging system consists of a 20× infinity corrected objective (Mitutoyo, Plan Apo NIR) with a working distance of 20 mm. The image is collected by a camera outside the vacuum vessel. In this configuration, shadowgraphy can be obtained, with a resolution of 1 µm (Fig. 5b). By adding a Wollaston prism (Small *et al*., 1973) and two polarizers outside the chamber, Nomarski-interferometry can be done to determine the electron density (Fig. 5c).

OUTLOOK

The double pulse setup described above was developed and implemented within the last year and has been used for experiments. More than 4000 shots on targets have been conducted so far, investigating changes in particle-energy distribution and proton beam profile. Tentative results show a clear dependence of particle energy and proton beam divergence on the spatial separation of the two foci. A detailed analysis and comparison to numerical simulations is currently under investigation and will be reported accordingly.

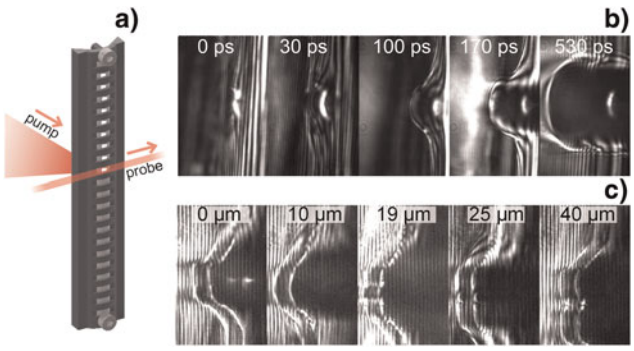

Fig. 5. (**a**) Curved target mount for transverse optical probing of the target rear surface. (**b**) High resolution shadowgraphy of an evolving plasma-plume, probed at different times compared to the pump-pulse. (**c**) Raw image by the Nomarski interferometric setup of two plasma-plumes for a fixed time but different separations, done by the split-mirror setup.

ACKNOWLEDGMENTS

We gratefully thank the Knut and Alice Wallenberg Foundation, the Swedish Research Council and the Swedish Foundation for Strategic Research for financial support. D. Neely acknowledges financial support by the UK Grant program: EP/K022415/1 (Advanced laser-ion acceleration strategies towards next generation healthcare).

REFERENCES

Aurand, B., Kuschel, S., Jäckel, O., Rödel, C., Zhao, H.Y., Herzer, S., Paz, A.E., Bierback, J., Polz, J., Elkin, B., Kamakar, A., Gibbon, P., Kaluza, M.C. & Kuehl, T. (2014). Enhanced radiation pressure-assisted acceleration by temporally tuned counter-propagating pulses. *Nucl. Inst. Meth. A* **740**, 033031.

Brenner, C.M., Green, J.S., Robinson, A.P.L., Carroll, D.C., Dromey, B., Foster, P.S., Kar, S., Li, Y.T., Markey, K., Spindloe, C., Streeter, M.J.V., Tolley, M., Wahlström, C.-G., Xu, M.H., Zepf, M., McKenna, P. & Neely, D. (2011). Dependence of laser accelerated protons on laser energy following the interaction of defocused, intense laser pulses with ultra-thin targets. *Lasers Part. Beams* **29**, 345–351.

Burza, M., Gonoskov, A., Genoud, G., Persson, A., Svensson, K., Quinn, M., McKenna, P., Marklund, M. & Wahlström, C.-G. (2011). Hollow microspheres as targets for staged laser-driven proton acceleration. *New J. Phys.* **13**, 013030.

Cartwright, B.G. & Shirk, E.K. (1978). A nuclear-track-recording polymer of unique sensitivity and resolution. *Nucl. Inst. Meth. A* **153**, 457–460.

Coury, M., Carroll, D.C., Robinson, A.P.L., Yuan, X.H., Brenner, C.M., Burza, M., Gray, R.J., Quinn, M.N., Lancaster, K.L., Li, Y.T., Lin, X.X., Tresca, O., Wahlström, C.-G., Neely, D. & McKenna, P. (2012). Influence of laser irradiated spot size on energetic electron injection and proton acceleration in foil targets. *Appl. Phys. Lett.* **100**, 074105.

Coury, M., Carroll, D.C., Robinson, A.P.L., Yuan, X.H., Brenner, C.M., Burza, M., Gray, R.J., Quinn, M.N., Lancaster, K.L., Li, Y.T., Lin, X.X., Tresca, O., Wahlström, C.-G., Neely, D. & McKenna, P. (2013). Injection and transport properties of fast electrons in ultra-intense laser-solid interactions. *Phys. Plasmas* **20**, 043104.

Daido, H., Nishiuchi, M. & S. Pirozhkov, S. (2012). Review of laser-driven ion sources and their applications. *Rep. Prog. Phys.* **75**, 056401.

Desforges, F.G., Hansson, M., Ju, J. Senje, L., Auder, T.L., Dobosz-Dufrenoy, S., Persson, A., Lundh, Wahlström, C.-G. & Cros, B. (2014). Reproducibility of electron beams from laser wakefield acceleration in capillary tubes. *Nucl. Instrum. Meth. A* **740**, 54–59.

Green, J., Borghesi, M., Brenner, C.M., Carroll, D.C., Dover, N.P., Foster, P.S., Gallegos, Pl., Green, S., Kirby, D., Kirkby, K.J., McKenna, P., Merchant, M.J., Najmudin, Z., Palmer, C.A.J., Parker, D., Prasad, R., Quinn, K.E., Rajeev,

https://doi.org/10.1017/S0263034614000779 Published online by Cambridge University Press

P.P., Read, M.P., Romagnani, L., Schreiber, J., Streetse, M.J.V., Tresca, O., Wahlström, C.-G., Zeft, M. & Neely, D. (2011). Scintillator-based ion beam profiler for diagnosing laser-accelerated ion beams. *SPIE Proc.* **8079**, 807991.

Hansson, M., Senje, L., Persso, A., Lundh, O., Wahlström, C.-G., Desforges, F.G., Ju, J., Audet, T.L., Cros, B., Dobosz, S. & Monot, P. (2014). Enhanced stability of laser wakefield acceleration using dielectric capillary tubes. *Phys. Rev. ST AB* **17**, 031303.

Hartmann, J. (1900). Bemerkungenüber den Bau und die Justirung von Spektrographen. *Z. Instrumentenkunde* **20**, 17–27, 47–58.

Hegelich, B.M., Albright, B.J., Cobble, J., Flippo, K., Letzring, S., Paffett, M., Ruhl, H., Schreiber, J., Schulze, R.K. & Fernández, J.C. (2006). Laser acceleration of quasi-monoenergetic MeV ion beams. *Nat.* **439**, 441–444.

Passoni, M., Bertagna, L. & Zani, A. (2010). Target normal sheath acceleration: Theory, comparison with experiments and future perspectives. *New J. Phys.* **12**, 045012.

Primot, J. & Sogno, L. (1995). Achromatic three-wave (or more) lateral shearing interferometer. *Z. JOSA A* **12**, 2679–2685.

Ramakrishna, B., Murakami, M., Borghesi, M., Ehrentraut, L., Nickles, P.V., Schürer, M., Steinke, S., Psikal, J., Tikhonchuk, V. & Ter-Avetisyan, S. (2010). Laser-driven quasimonoenergetic proton burst from water spray target. *Phys. Plasmas* **17**, 083113.

Robson, L., Simpson, P.T., Clarke, R.J., Ledingham, K.W.D., Lindau, F., Lundh, O., McCanny, T., Mora, P., Neely, D., Wahlström, C.-G.,, Zepf, M. & McKenna, P. (2007). Scaling of proton acceleration driven by petawatt-laser plasma interactions. *Nat. Phys.* **3**, 58–62.

Ruprecht, A.K., Pruss, C., Tiziani, H.J., Wolfgan, O., Peter, L., Arndt, L., Mohr, J. & Lehmann, P. (2005). Confocal micro-optical distance sensor: Principle and design. *Z. SPIE Proc.* **5856**, 128–135.

Schreiber, J., Bell, F. Grüner, F., Schramm, U., Geissler, M., Schnüger, Ter-Avetisyan, S., Hegelich, B.M., Cobble, J., Brambrink, E., Fuchs, J., Auderbert, P. & Habs, D. (2006). Analytical model for ion acceleration by high-intensity laser pulses. *Phys. Rev. ST AB* **97**, 045005.

Schwoerer, H., Pfotenhauer, S. Jäckel, O., Amthor, K.-U., Liesfeld, B., Ziegler, W., Sauerbrey, R., Ledingham, K.W.D. & Esirkepov, T. (2006). Laser-plasma acceleration of quasi-monoenergetic protons from microstructured targets. *Nat.* **439**, 445–448.

Small, R.D., Sernas, V.A. & Page, R.H. (1972). Single beam Schlieren interferometer using a Wollaston prism. *Appl. Opt.* **11**, 858–862.

Strickland, D. & Mourou, G. (1985). Compression of amplified chirped optical pulses. *Opt. Commun.* **56**, 219–221.

Tresca, O., Carroll, D.C., Yuan, X.H., Aurand, B., Bagnoud, V., Brenner, C.M., Coury, M., Fils, J., Gray, R.J., Kühl, T., Li, C., Li, Y.T., Lin, X.X., Quinn, M.N., Evans, R.G., Zielbauer, B., Roth, M., Neely, D. & McKenna, P. (2011). Controlling the properties of ultra-intense laser proton sources using transverse refluxing of hot electrons in shaped mass-limited targets. *Plasma Phys. Contr. Fusion* **53**, 105008 .

Wilks, S.C., Langon, A.B., Cowan, T.E., Roth, M., Singh, M., Hatchett, S., Key, M.H., Pennington, D., MacKinnon, A. & Snaverly, R.A. (2001). Energetic proton generation in ultra-intense laser solid interactions. *Phys. Plasmas* **8**, 542–549.

https://doi.org/10.1017/S0263034614000779 Published online by Cambridge University Press